Entropic Lattice Boltzmann Method for Multiphase Flows

A. Mazloomi M, S. S. Chikatamarla, and I. V. Karlin

Department of Mechanical and Process Engineering, ETH Zurich, 8092 Zurich, Switzerland
(Received 24 September 2014; published 1 May 2015)

A novel thermodynamically consistent lattice Boltzmann model that enables dynamical effects of two-phase fluids is developed. The key innovation is the application of the entropic lattice Boltzmann stabilization mechanism to control the dynamics at the liquid-vapor interface. This allows us to present a number of simulations of colliding droplets, including complex phenomena such as the formation of a stable lamella film. Excellent agreement of the simulation with recent experiments demonstrates the viability of the present approach to simulation of complex dynamic phenomena of multiphase fluids.

Multiphase fluid flows are ubiquitous in science and technology and have received considerable attention [1]. The interplay between the interface dynamics and the surrounding fluid motion is subtle, with factors such as density and temperature jumps across the interface, surface-tension effects, topological connectivity, and boundary conditions playing a significant role in the dynamics [2]. While experimental studies of multiphase phenomena are greatly improving [3], the existing computational methods remain hindered by complex implementations and lack of tools to accurately describe the physical phenomenon behind multiphase flows. Conventional methods of simulating multiphase flows based on continuum mechanics equations or molecular dynamics lack either thermodynamic consistency or computational efficiency or both, and hence cannot be used as reliable tools to advance this complex field. Apart from computational cost, such techniques require complex implementations (grid refinement, etc.) even for the simplest cases [4,5].

Recently, the mesoscopic lattice Boltzmann method followed a much different path to complex flow phenomena [6]. It is thus not surprising that LB methods were advocated as a possible alternative for the simulation of fluids undergoing phase transition by a number of authors [7,8]. However, LB methods still suffer from substantial drawbacks such as restriction on the kinematic viscosity, interface thickness, low density ratio between the liquid and vapor phases, and others. In spite of a number of refinements (see review, e.g., [9,10] and references therein), existing LB formulations for the multiphase flows are still unable to address complex dynamical effects, such as droplet collisions, in a quantitative fashion. Moreover, many of the attempts at improving the performance of multiphase models were concentrated around simplifying existing approaches by sacrificing the physics of the model [11,12] or resorting to improvements on Shan-Chen type models, where one cannot introduce temperature that is consistent with thermodynamics [7,13–15].

In this Letter, we propose a novel thermodynamically consistent lattice Boltzmann model for two-phase flow simulations free of the above limitations. Key is the use of the entropic lattice Boltzmann method (ELBM), together with the optimal choice of the equation of state. A number of results on droplet collisions are presented and compared with experimental data, including a complex lamella film stabilization. Our results demonstrate that the novel formulation is suitable for realistic multiphase studies.

The classical capillarity theory, for multiphase flows, by van der Waals [16] and Korteweg [17] (see, e.g., [18] and references therein) is followed below. The free-energy functional is composed of a bulk free energy, Ψ, and an excess free energy stored at the liquid-vapor interface,

$$F = \int \left[\Psi(\rho) + \frac{\kappa}{2}|\nabla\rho|^2 \right] d\boldsymbol{x}, \qquad (1)$$

where κ is the surface tension coefficient and ρ is the local density. Equation (1) implies Korteweg's stress [17],

$$\boldsymbol{P} = \left(p - \kappa\rho\nabla^2\rho - \frac{\kappa}{2}|\nabla\rho|^2 \right)\boldsymbol{I} + \kappa(\nabla\rho) \otimes (\nabla\rho), \quad (2)$$

where p is the equation of state (EOS), $p = \rho(d\Psi/d\rho) - \Psi$, and $\boldsymbol{I}$ is the unit tensor. Implementation of Korteweg's stress (2) in the lattice Boltzmann setting, the so-called free-energy LB model, was first suggested by Swift, Osborn, and Yeomans [8], and refined by Wagner and Li [19]. In the forcing method of implementation of multiphase models, the local flow velocity is altered by an amount $\delta\boldsymbol{u} = (\boldsymbol{F}/\rho)\delta t$, where $\delta t = 1$ is the lattice time step, and $\boldsymbol{F}$ is the force related to Korteweg's stress,

$$\boldsymbol{F} = \nabla \cdot (\rho c_s^2 \boldsymbol{I} - \boldsymbol{P}), \qquad (3)$$

where c_s^2 is the lattice speed of sound. However, existing realizations do not allow for significant density ratios between liquid and vapor phases, small kinematic viscosity,

and are unstable for simulation of droplet dynamics. Hence, a reformulation is required.

The major restyling here is to use the entropic lattice Boltzmann method (ELBM) [20],

$$f_i(\mathbf{x} + \mathbf{v}_i, t + 1) - f_i(\mathbf{x}, t) = \alpha\beta[f_i^{\mathrm{eq}}(\rho, \mathbf{u}) - f_i(\mathbf{x}, t)]$$
$$+ [f_i^{\mathrm{eq}}(\rho, \mathbf{u} + \delta\mathbf{u}) - f_i^{\mathrm{eq}}(\rho, \mathbf{u})], \tag{4}$$

where $0 < \beta < 1$ is a parameter related to the kinematic viscosity, $\nu = \mu/\rho = (\beta^{-1} - 1)c_s^2/2$ and strictly following the free energy formulation of the multiphase models that ensure thermodynamic consistency. The equilibrium f^{eq} is the minimizer of the discrete entropy function H under the constraints of local conservation laws of mass and momentum, $\{\rho, \rho\mathbf{u}\} = \sum_i \{1, \mathbf{v}_i\}\{f_i^{\mathrm{eq}}\}$, where

$$H = \sum_i f_i \ln(f_i/W_i), \tag{5}$$

with W_i the lattice-specific weights. For the sake of computational efficiency, it suffices to use the expansion of the minimization problem to order u^3,

$$f_i^{\mathrm{eq}} = \rho W_i \left(1 + \frac{v_{i\alpha} u_\alpha}{c_s^2} + \frac{u_\alpha u_\beta}{2c_s^4}(v_{i\alpha} v_{i\beta} - c_s^2 \delta_{\alpha\beta}) \right.$$
$$\left. + \frac{u_\alpha u_\beta u_\gamma}{6c_s^6} v_{i\gamma}(v_{i\alpha} v_{i\beta} - 3c_s^2 \delta_{\alpha\beta}) \right). \tag{6}$$

A key point is the parameter α in Eq. (4) that maintains the entropy balance in the relaxation step at each node, and is available as the nontrivial root of the equation,

$$H[f + \alpha(f^{\mathrm{eq}} - f)] = H(f). \tag{7}$$

The last term on the right-hand side of Eq. (4) is a specific realization of the forcing (in the ELBM setting, it was used in [21] for gravity force).

To this end, the difference from the standard LB models for the two-phase flow is the ELBM relaxation [α is computed from the entropy balance (7), as opposed to taking the fixed value $\alpha = 2$]. Originally, ELBM was conceived for the stabilization of high Reynolds number flow simulations to handle large velocity gradients. There, fluctuations of α around $\alpha = 2$ due to the entropy estimate Eq. (7) acts as a built-in turbulence model. However, in multiphase flows, ELBM stabilizes the simulation through control of spurious currents arising from the transport of the fictitious "molecules" that carry net momentum across the interface (unlike real molecules, which achieve equilibrium through fluctuations across the interface without carrying net momentum) [22,23]. Also, ELBM maintains the large density gradients present in a multiphase flow, for example, near a liquid vapor interface, which otherwise are a major source of instabilities. This problem was partially averted

by introducing diffuse interfaces [24]; however, this is not a viable solution for flows with a large number of droplets or flows with small droplet sizes.

Finally, it remains to specify the EOS p. To that end, we use a polynomial equation of state so chosen as to match the Peng-Robinson (PR) equation of state [25]. Polynomial equation of states have long been used in the literature as an alternative to the realistic equation of states which are a fit of the experimental data in different regimes.

$$p = \rho R_G T(1 + b\rho\chi) - a\rho^2, \tag{8}$$

where χ is the density-dependent collision probability [26], considered here as a polynomial in density, $\chi = \sum_{k=0}^4 A_k \rho^k$, where, in turn, functions A_k are a polynomials of the temperature, $A_k = \sum_{n=0}^6 a_{kn} T^n$. Numerical values of the coefficients in these polynomials are given in the Supplemental Material [27] along with implementation details. In the simulations we set $a = 9/49$, $b = 2/21$ and $R_G = 1$. We note that, restoring to an EOS of a polynomial form proves advantageous with respect to the nonpolynomial PR EOS, since it avoids singularities, and greatly improves the performance of the present model.

Simulations were performed using the standard 19-velocity lattice, $c_s^2 = 1/3$, and weights W_i can be found in the Supplemental Material [27]. The thermodynamic consistency of the present model was validated numerically by simulating the coexistence curve as shown in Fig. 1. It can be seen that the densities of the liquid and vapor phases in the simulation agree well with the values predicted by Maxwell's equal area rule. The maximal density ratio $r = \rho_l/\rho_v$ of the liquid and vapor phases achieved in these simulations was $r > 800$. Free energy models, by construction, allow the surface tension of the liquid-vapor interface to be controlled independently of the grid size and the viscosity. This is demonstrated in Fig. 2, where it is shown that by changing the surface tension coefficient κ we obtain the value of the surface tension independent of the
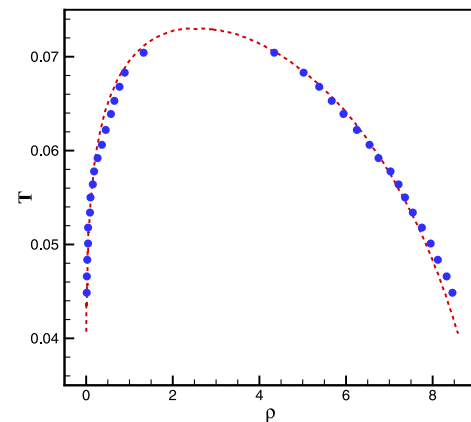

FIG. 1 (color online). The coexistence curve. Symbol: ELBM simulation; Line: Maxwell's equal area rule.
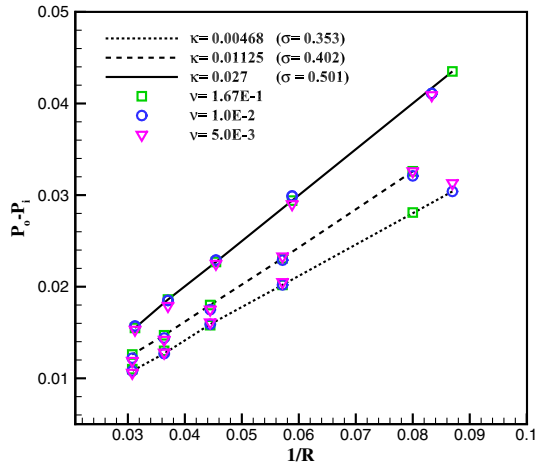
FIG. 2 (color online). Laplace's law for various values of viscosity and surface tension coefficient κ. As expected, with the increasing κ, the surface tension σ increases independent of the viscosity. The liquid and vapor densities are $\rho_l = 7.82$, $\rho_v = 0.071$, respectively.

viscosity. It is evident that the pressure difference between the liquid and vapor phases in a droplet is inversely proportional to the radius of the droplet (Laplace's law, $\Delta P = \sigma/R$, where σ is the surface tension). In addition to that, we observed that the magnitude of spurious currents in the vicinity of the droplet does not scale with the kinematic viscosity, and was maintained at $\sim 10^{-3}$–10^{-2} (grid units) in a range of low kinematic viscosity $\nu \sim 10^{-2}$–10^{-4}. Thus, the typical spurious currents in the present ELBM realization are more than an order of magnitude smaller than the typical velocity of the liquid $U \sim 0.1$. The problem of spurious currents together with low density ratios restricted the application of free energy models to stationary droplets suspended in vapor or sitting on a surface. However, the present model easily overcomes these problems and can be extended to study dynamical effects such as droplet collisions. It must be mentioned that the standard LBGK model goes unstable at fluid viscosities below $\nu = 1.5 \times 10^{-2}$, while the entropic LBM remains stable beyond $\nu < 10^{-5}$ for the same lattice. The droplet collision phenomenon leads to many interesting stability and topological configurations. Droplet collisions are controlled primarily by the Reynolds number Re, the Weber number We, and the impact parameter γ, $\mathrm{Re} = UD_-/\nu_l$, $\mathrm{We} = \rho_l U^2 D_-/\sigma$, $\gamma = 2B/(D_- + D_+)$, with D_- and D_+ the diameters of the smaller and of the larger droplets, U the relative velocity at impact, B the offset between the droplet centers, and ν_l the viscosity of the liquid phase. Figure 3 shows various configurations during a collision of equal sized droplets separated by a small offset. Excellent agreement is obtained by the current model with respect to the experiments of Qian and Law [28]. In Fig. 4 experimental and present simulation snapshots at various stages of collision of unequal sized droplets are compared. The experiments of Tang, Zhang, and Law [29] captured
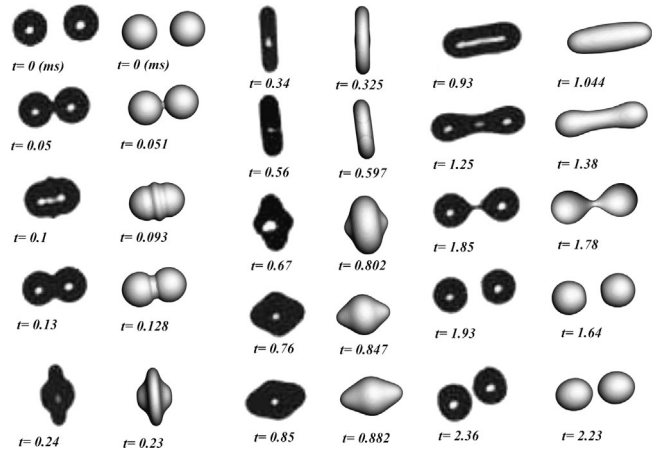

FIG. 3. Sequence of coalescence observed for binary collision of equal size droplet at We $= 37.2$, Re $= 228.0$, $\gamma = 0.01$, and $D = 328$ μm. Left: Experiment [28]. Right: Simulation.

the shapes in a head-on collision, which compare very well with the present simulations. Grid sizes for these simulations are $150 \times 150 \times 150$ and $245 \times 105 \times 105$, respectively.

In order to illustrate the significance of the ELBM formulation, we show a snapshot of the computed relaxation parameter α at a particular instance of droplets collision (see Fig. 2 in the Supplemental Material [27]). As expected, significant deviation of α from $\alpha = 2$ is observed at the interface only. This provides evidence that the ELBM performs effective control at the interface. Even though ELBM scheme comes at an added computational cost in the form of the evaluation of entropy estimate [solving Eq. (7) at each grid node], which for a typical simulation is a factor 3 to 4 as compared to LBGK; the saving in grid sizes (typically an order of magnitude smaller grid resolution in each spacial dimension) makes the computations extremely efficient.
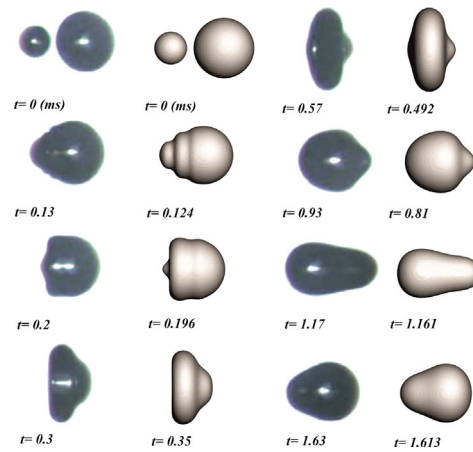

FIG. 4 (color online). Comparison of the dynamics of a head-on collision between two droplets of unequal size. Left: Experiment [29]; Right: Simulation. We $= 17.6$, Re $= 185.0$, $\gamma = 0.0$, $D_- = 100$ μm, and $D_+ = 187$ μm.
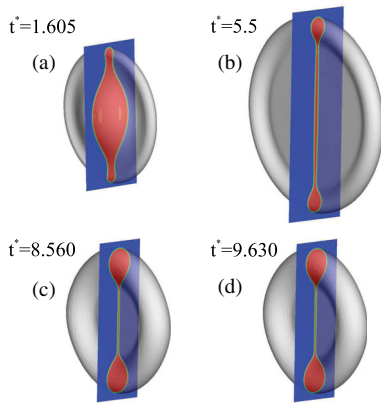
FIG. 5 (color online).   Different stages of lamella stabilization simulation at We = 269 and Re = 154. (a),(b): Expansion of the lamella; (c),(d): Contraction of the lamella.

Perhaps one of the most interesting droplet collision experiments was performed by Willis and Orme [30]. When two equal sized droplets collide head-on, a very thin film known as the lamella film is formed during the deformation processes [30]. Depending on the Weber number, the lamella can either remain attached to the rim of the droplet or rupture and detach from it. Figure 5 shows snapshots at four nondimensional times $t^* = tU/D$ for the simulation of stable lamella (we do not show here the initial stages of droplet collision like in Fig. 3). Remarkably, the present model captures the thin lamella film which is just two to three grid spacings thick. Conventional methods for multiphase flows face severe numerical constraints in simulating this problem due to large grid requirements needed to resolve the thin film formed. Moreover, inaccuracies in the grid refinement can lead to oscillations in the flow field that rupture the lamella film. The simplicity, efficiency, and accuracy of the present model is well tested and demonstrated through these comparisons. Figure 6 shows the comparison of the maximum diameter of the merged droplets in both
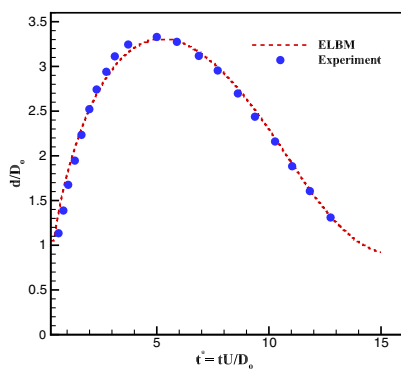
experiments and present simulations. Excellent comparison between experiment and simulation is evident.

The proposed model, however, is limited to isothermal problems where the temperature dynamics are not considered; further extensions in the spirit of Ref. [31] are planned for the future. Also, it must be mentioned that with the limited resolution used here, very high We and Re number applications such as high speed sprays are not yet possible.

To conclude, we have demonstrated that the proposed modifications to the free-energy based lattice Boltzmann models bring about a substantial increase in the operating range of multiphase simulations. The new model proposed drastically increases the liquid-vapor density ratio and decreases the minimal viscosity in multiphase simulations. Also, for the first time, accurate and reliable results were obtained for nonstationary droplets using the free energy formulation that assures thermodynamic consistency and deep physical insights into the flow field. The entropic lattice Boltzmann method was successfully employed to achieve high Reynolds number and high Weber numbers that are typical for two-phase applications. Further simulations with new wall boundary conditions are underway and will be reported elsewhere.

FIG. 6 (color online).   Comparison of the maximum radial deformation measured from ELBM simulations (line) and experimental data [30] (symbol) at We = 269, Re = 154, and $D = 516 \ \mu$m.

[1] C. E. Brennen, *Fundamentals of Multiphase Flow* (Cambridge University Press, Cambridge, England, 2005).
[2] D. A. Drew, Annu. Rev. Fluid Mech. **15**, 261 (1983).
[3] Y. Liu, L. Moevius, X. Xu, T. Qian, J. M. Yeomans, and Z. Wang, Nat. Phys. (London) **10**, 515 (2014).
[4] J. Sethian and P. Smereka, Annu. Rev. Fluid Mech. **35**, 341 (2003).
[5] Y. Sui, H. Ding, and P. Spelt, Annu. Rev. Fluid Mech. **46**, 97 (2014).
[6] S. Succi, *The Lattice Boltzmann Equation for Fluid Dynamics and Beyond* (Oxford University Press, Oxford, 2001).
[7] X. Shan and H. Chen, Phys. Rev. E **47**, 1815 (1993).
[8] M. R. Swift, W. R. Osborn, and J. M. Yeomans, Phys. Rev. Lett. **75**, 830 (1995).
[9] C. K. Aidun and J. R. Clausen, Annu. Rev. Fluid Mech. **42**, 439 (2010).
[10] R. Nourgaliev, T. Dinh, T. Theofanous, and D. Joseph, Int. J. Multiphase Flow **29**, 117 (2003).
[11] H. W. Zheng, C. Shu, and Y.-T. Chew, J. Comput. Phys. **218**, 353 (2006).
[12] T. Lee and C. Lin, J. Comput. Phys. **206**, 16 (2005).
[13] Q. Li, K. H. Luo, and X. J. Li, Phys. Rev. E **87**, 053301 (2013).
[14] H. Huang, J.-J. Huang, X.-Y. Lu, and M. C. Sukop, Int. J. Mod. Phys. C **24**, 1350021 (2013).

[15] M. Sbragaglia, R. Benzi, L. Biferale, S. Succi, K. Sugiyama, and F. Toschi, Phys. Rev. E **75**, 026702 (2007).

[16] J. D. van der Waals, Verhand. Kon. Akad. V Wetensch. Amst. (Sect. 1) **1(8)**, 1 (1893).

[17] D. J. Korteweg, Arch. Neerl. Sci. Exactes Nat. Ser. II **6**, 1 (1901).

[18] M. Slemrod, J. Diff. Equ. **52**, 1 (1984).

[19] A. J. Wagner and Q. Li, Physica (Amsterdam) **362A**, 105 (2006).

[20] I. V. Karlin, A. Ferrante, and H. C. Öttinger, Europhys. Lett. **47**, 182 (1999).

[21] S. S. Chikatamarla and I. V. Karlin, Physica (Amsterdam) **392A**, 1925 (2013).

[22] C. M. Pooley and K. Furtado, Phys. Rev. E **77**, 046702 (2008).

[23] K. Connington and T. Lee, J. Mech. Sci. Tech. **26**, 3857 (2012).

[24] D. Lycett-Brown, K. H. Luo, and W. Liu, Phys. Fluids **26**, 023303 (2014).

[25] P. Yuan and L. Schaefer, Phys. Fluids **18**, 042101 (2006).

[26] X. He and G. D. Doolen, J. Stat. Phys. **107**, 309 (2002).

[27] See Supplemental Material at http://link.aps.org/supplemental/10.1103/PhysRevLett.114.174502 for details of the implementation of the present entropic lattice Boltzmann model.

[28] J. Qian and C. K. Law, J. Fluid Mech. **331**, 59 (1997).

[29] C. Tang, P. Zhang, and C. K. Law, Phys. Fluids **24**, 022101 (2012).

[30] K. Willis and M. Orme, Exp. Fluids **34**, 28 (2003).

[31] R. Zhang and H. Chen, Phys. Rev. E **67**, 066711 (2003).